Journal of Metals, Materials and Minerals, Vol. 31, No. 3, pp. 70-84, 2021

Effect of cladding of stellite-6 filler wire on the surface of SS316L alloy through cold metal arc transfer process

Thinesh Babu THIAGARAJAN[1,*], and Sengottuvel PONNUSAMY[1]

[1] *Bharath Institute of Higher Education and Research, Chennai 600073 India*

***Corresponding author e-mail:** thineshbabu@outlook.com

Received date:
6 July 2021
Revised date
6 August 2021
Accepted date:
12 August 2021

Keywords:
Cladding;
CMT;
Stellite-6;
SEM-EDAX;
Vickers-hardness

Abstract

In this work, Cladding was done on SS316L alloy through the CMT process using Stellite-6 filler wire. 31 experiments were done at different welding conditions as per CCD matrix. The cladding specimens were characterized by macro and micro-study, Vickers microhardness evaluation and corrosion resistance analysis. An optical microscope, SEM-EDAX, and XRD were used to predict the structural characterizations, presence and the distributions of the elements. Based on the study higher voltage and welding speed showed appreciable hardness at the interface & cladding regions. The thickness of the interface was noted at a maximum of 190 μm. The EDS spectra showed that Fe, Cr and Co were the major elements in the clad and interface regions. The Co-rich phase and the low content of element O are found in the low corroded regions on the specimen. The maximum hardness observed at cladding and interface were 378 Hv and 270 Hv respectively.

1. Introduction

In industries, the insufficient tribological, mechanical and corrosion properties of materials can confine their applications in many areas. To overcome these limitations, many advanced surface modifications like coating, cladding have emerged with the help of welding processes like CMT, Laser [1-3], and tungsten inert gas (TIG), etc. [4]. The hybrid cladding process can improve the deposition efficiency, but controlling the process may be difficult [5]. According to Gabriel T. *et al.* [6], laser cladding makes micron level coating on the substrates and by modifying the laser power the cladding efficiency can be varied. The cladding process with high speed laser improves the cladding efficiency than the low speed laser [7]. The laser cladding accuracy is appreciated. Wang K *et al.* [8] made chromium alloy based coating on copper alloy substrate using pulse laser induction cladding process and proved the increase of wear property. TIG cladding has the advantages of low solidification time and narrow HAZ. Plasma transferred arc cladding produces no distortion and improves wear properties [9]. Friction cladding is a solid state eco-friendly cladding compared to CMT. CMT is an advanced version of metal inert gas (MIG) welding [10]. The welding mechanism of the MIG process is shown in Figure 1(a). The metal is deposited through the wire electrode over the substrate. The mechanism of transferring molten stage metal affects the weld performance as some of the forces are involved as mentioned in Figure 1(a). The electromagnetic force (pinch) is applied regularly on the conductor and increases proportionally to the square of the current and decreases to the square of the cross-sectional area of filler wire. Figure 1(b) is the CMT process's metal deposition mechanism. In the initial stage, the filler wire moves towards to weld pool. Then the arc stopped when the wire entered the weld pool. As a third step, the filler wire gets back to detach the metal drops. Thus the process is repeating. It can be used for thick materials. It employs a consumable wire that acts as both the electrode and the filler material. The heat input required to CMT is lesser than that of the MIG process. In CMT cladding, a metal is deposited on another substrate material. The performance of the cladding can be controlled by varying the process parameters. A literature study shows the increase in depth of penetration and bead when the welding current increases. The welding current plays a vital role. Stellite-6 alloy is widely popular in the cladding process as the alloy has appreciable wear and corrosion property and thus many works have been done by the researchers. Gholipour *et al.* [11] studied the structural and wear properties of 17-PH stainless steel cladding with stellite 6 filler wire. The study discussed the phases formed in the cladding and the surface layer contents. The surface layer had the carbides with dendrite microstructure [12]. The hardness results showed an increase towards the coating surface from the interface. It was noted during the wear test that when the surface temperature increases it showed the formation of the phase of Cr_2O_3. Guojian Xu *et al.* [13] comparatively studied the stellite-6 cladding performance on SS403 alloy by laser diode process and TIG process. Through the research, it was found that laser cladding process performance was good. Laser cladding had a lower dilution and lower specific wear rate and they recommend laser cladding for the narrow HAZ with high hardness. Kumaran *et al.* [14] mentioned that the gas metal arc welding produced cracks in the welding of aluminium, and used the CMT process to overcome such crack problems. The authors

made butt joints for the comparative study on AA7475 alloy using normal and pulsed CMT processes. Pulsed CMT yielded maximum joint efficiency. Brownlie *et al.* [15] studied the cladding on carbon steel with lost wax cast satellite-6 and compared the results with stainless steel (SS). The results showed that the satellite-6 cladding was better than the SS. Alain Kusmoko *et al*. [16] did stellite-6 cladding on medium carbon steel using laser cladding and found fewer cracks on the specimens which were coated by lower heat input. C.R.C Lima *et al.* [17] compared the corrosion and wear property of stellite-6 cladding by TIG and high-velocity oxygen fuel (HVOF) process and found HVOF was having better wear resistance and TIG had better corrosion and erosion results. Through the literature survey, it is noted that stellite-6 and SS316L alloy are good in the cladding process and much work was done on them especially in Laser cladding. Also, the research of stellite-6 and SS316L CMT cladding is limited.

In this work, an attempt was tried to investigate the performance of the CMT process and the effect of stellite cladding on SS316L alloy. The novelty of the work is to utilize the cold metal arc transfer which is an advanced technique of gas metal arc welding (GMAW) for the metals like stellite-6, SS316L at the welding conditions derived based on a central composite design matrix with four factors. This cladding study is helpful overcome the issues on the life of pipes and fittings used in marine, and refineries applications.

2. Materials and Methods

2.1 Materials

For the cladding experiments, the SS316L alloy was used as a substrate and stellite-6 was used as a filler wire for cladding material in the experiments. The chemical composition of the base metal and filler wire is given in Table 1. Stellite is one of the cobalt-based two-phase alloys [2,18]. Due to its excellent erosion resistance [19] and wear resistance property [1], this material is considered as a choice for making the components where the wear and corrosion resistance without compromising the strength are highly recommended in the higher temperature atmosphere [20]. Stellite material is widely used in industries for fabricating lathe machine tool, Saw teeth, machine parts, valves for IC engines, and bone replacement in medical applications. The stellite-6 properties can be further improved by the element additions, by increasing the layers count or some of the metal pressed processes [21]. SS316L alloy is a kind of low carbon austenitic stainless steel and its weldability is good in the cladding welding process [22]. The wear property of SS316 alloy can be improved by the nano coating using cladding process [23]. It is widely popular among aerospace, marine and household applications due to its excellent corrosion resistance property. The acetone was used to cleanse the surfaces of the specimen to remove dirt and grease during welding.

2.2 Method

In this work, CMT Welding Process was used for depositing the co-based Stellite-6 alloy over the surface of SS316L alloy according to the different conditions of welding current, voltage, torch angle and welding speed as shown in Table 2 as discussed through Figures 1(a) and (b). The welding matrix was set based on the central composite design (CCD) [24] concept for the optimization of process parameters. In this study, CCD is used for standardizing the experiments and to obtain the optimum values. It is a factorial design and is helpful for sequential experiments and the optimal processing variables [25]. As a second order response surface model, three types of design points are there like center points, axial and factorial [26]. Improper selection of welding parameters leads to having a crack and some unwanted outputs [27]. The weld condition matrix is shown in Table 3. CCD is, a branch of response surface methodology (RSM) used for the optimization of the cladding process [28], a tool to solve complex engineering problems with required experimental runs [29,30]. The stellite-6 filler rod of ϕ1.2 mm diameter was used. The SS316L plate dimension was 200 mm × 420 mm. The prepared specimens were cut by an EDM machine and polished as needed for the characterization using aqua regia etchant. The performance of the clad specimens was investigated through various characterizations like macrographs and microstructures to study the cladding interfaces through an optical microscope (Model: Dewinter optical tech) and scanning electron microscope attached with EDS set up (Model: Geminis SEM 300, Carlzeiss), XRD analysis to identify the phases, elemental distributions through EDS spectra at weld interface and base metal regions, Vickers microhardness study along with the base metals and the clad interface, and corrosion resistance analysis. The microhardness was measured using Vickers hardness tester (Model: INNOVATEST) with a 1 kg load and 10 s dwell time. Corrosion was studied through the method of potentiodynamic polarization [31] (Model: Electrochemical impedance-CHI660 A).

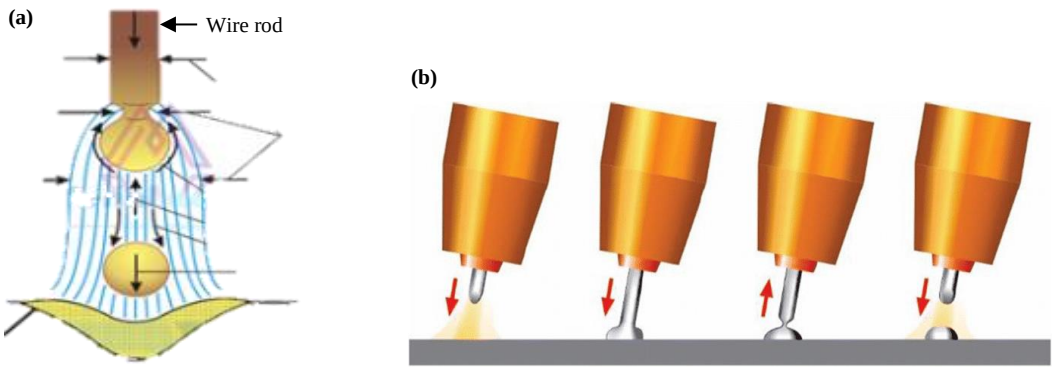

Figure 1. MIG welding mechanism (a) and CMT metal deposition (b).

Table 1. Chemical composition of metals (elements in wt%).

Base material: SS316L									
C	Mn	Si	Cr	Ni	Mo	P	S	N	Fe
0.03	2	0.75	16-18	10-14	2-3	0.045	0.03	0.1	Bal.
Filler wire: Stellite 6									
Cr	W	C	Fe	Si	Mn	Co			
28	4	1.15	1.3	1.1	0.06	Bal.			

Table 2. Welding parameters and their levels.

Parameters	**Notation**	**-2**	**-1**	**0**	**+1**	**+2**
Welding current (A)	I	120	140	160	180	200
Voltage (v)	V	15	17	19	21	23
Torch angle (deg)	TA	50	60	70	80	90
Welding speed ($m \cdot min^{-1}$)	TS	100	125	150	175	200

Table 3. Welding conditions matrix for the experiments as per CCD.

Exp. no.	**I (A)**	**V (V)**	**TA (deg)**	**TS ($m \cdot min^{-1}$)**	**Exp. no.**	**I (A)**	**V (V)**	**TA (deg)**	**TS ($m \cdot min^{-1}$)**
1	140	17	60	125	17	120	19	70	150
2	180	17	60	125	18	200	19	70	150
3	140	21	60	125	19	160	15	70	150
4	180	21	60	125	20	160	23	70	150
5	140	17	80	125	21	160	19	50	150
6	180	17	80	125	22	160	19	90	150
7	140	21	80	125	23	160	19	70	100
8	180	21	80	125	24	160	19	70	200
9	140	17	60	175	25	160	19	70	150
10	180	17	60	175	26	160	19	70	150
11	140	21	60	175	27	160	19	70	150
12	180	21	60	175	28	160	19	70	150
13	140	17	80	175	29	160	19	70	150
14	180	17	80	175	30	160	19	70	150
15	140	21	80	175	31	160	19	70	150
16	180	21	80	175					

3. Results and discussion

All the specimens were tested and the results are presented here. The parameters like depth of penetration, a width of bead, weld toe angle and face reinforcement all are evaluated for each experiment. Table 4 furnishes the values obtained through this investigation. The depth of penetration was more and a maximum of 3.1 mm for the 10th experiment with a maximum of current and welding speed. But from the result, it was observed that the welding speed and the current values were influencing the depth of penetration majorly as they decrease the penetration was also decreased. A maximum of 13.5 mm bead width was observed for the 11th experiment with the welding conditions of low current & torch angle and high voltage and welding speed. Here the voltage was the deciding authority for the width of the weld bead. According to the results, if the voltage decreases, then the width of the bead also decreases. Similarly, the weld toe angle range was 64° to 116° with a maximum for the 11th experiment. Generally, the welding speed is the important one while cladding. The value of weld toe angle was varied depending on the weld conditions. The 22nd experiment had a low weld toe angle with a maximum of a torch angle of 90°; the low torch angle yielded a high toe angle.

Figure 2(a-c) shows the results for all the experiments in the case of interface thickness, weld area and K-ratio respectively. The 'K' vale was calculated based on the ratio of the width of the bead to the depth of penetration. From Figure 2(a) the clad interface thickness can be understood. The thickness was in the range of 0.048 mm to 0.19 mm. The thin interface was recorded for 23rd and 27th experiments and the maximum value was recorded for the 26th experiment with 19 V. it was noted that the low welding speed decreases the interface thickness while comparing the values of the 23rd and 26th experiments. Figure 2(b), consolidated the values of the weld area. The maximum and minimum weld area of 54.8 mm^2 and 19 mm^2 was obtained for the 11th and 2nd experiment respectively. High voltage and higher welding speed produced higher weld area. When the voltage value decreased the weld area was also decreased. From these results obtained, it was found that the voltage and welding speed was the determining parameters for the weld area. Figure 2(c) is the plot of the K-ratio. The parameters like depth of penetration during the cladding and the width of bead obtained are the deciding parameters for the 'K'

values. The estimated values were compared among all the experiments. It was observed from the plot that the combinations such as higher current with a low volt or low current with a high volt increased the K ratio. A maximum value was recorded as 5.0 for the 11th experiment with 140 A and 21 V, whereas the minimum of 2.6 for the 4th experiment that had low speed 125 m·min^{-1}, current 180 A and 21 V. Though it was difficult to judge the influencing parameter in case of K ratio, the low weld speed may be the reason for the low K ratio as per the results.

Table 4. Result observed for the experiments.

Exp. No.	Observed parameters				Exp. No.	Observed parameters			
	A	B	C	D		A	B	C	D
1	2.744	7.853	3.059	100.08	17	2.318	7.567	2.676	65.447
2	1.625	7.049	2.477	100.578	18	2.310	7.379	2.763	69.274
3	2.200	7.900	2.900	101.235	19	2.693	8.078	2.898	69.615
4	2.886	7.854	3.140	103.132	20	2.420	7.720	2.984	65.464
5	2.271	7.380	2.965	101.434	21	2.335	7.601	2.779	71.250
6	2.900	8.500	3.200	99.531	22	1.875	6.937	2.454	64.680
7	2.100	8.300	2.800	100.356	23	2.096	7.056	2.556	70.351
8	2.713	7.430	3.092	98.056	24	1.926	7.295	2.985	78.574
9	2.460	7.807	2.635	100.783	25	2.234	7.159	3.188	88.781
10	3.170	8.563	3.628	98.016	26	1.944	7.006	2.966	85.012
11	2.624	13.463	4.236	116.316	27	1.977	6.834	2.949	94.021
12	2.028	7.635	2.352	76.481	28	1.994	7.092	2.642	66.801
13	2.114	7.311	2.591	62.868	29	1.755	6.922	3.170	87.841
14	1.704	7.721	3.119	90.531	30	1.995	7.005	2.848	89.340
15	2.437	7.533	2.890	79.247	31	1.858	7.618	3.597	86.203
16	2.574	7.910	5.711	77.406					

* where, A- Depth of Penetration (mm), B- Width of Bead (mm), C- Face Reinforcement (mm), D- Weld Toe Angle (degree).

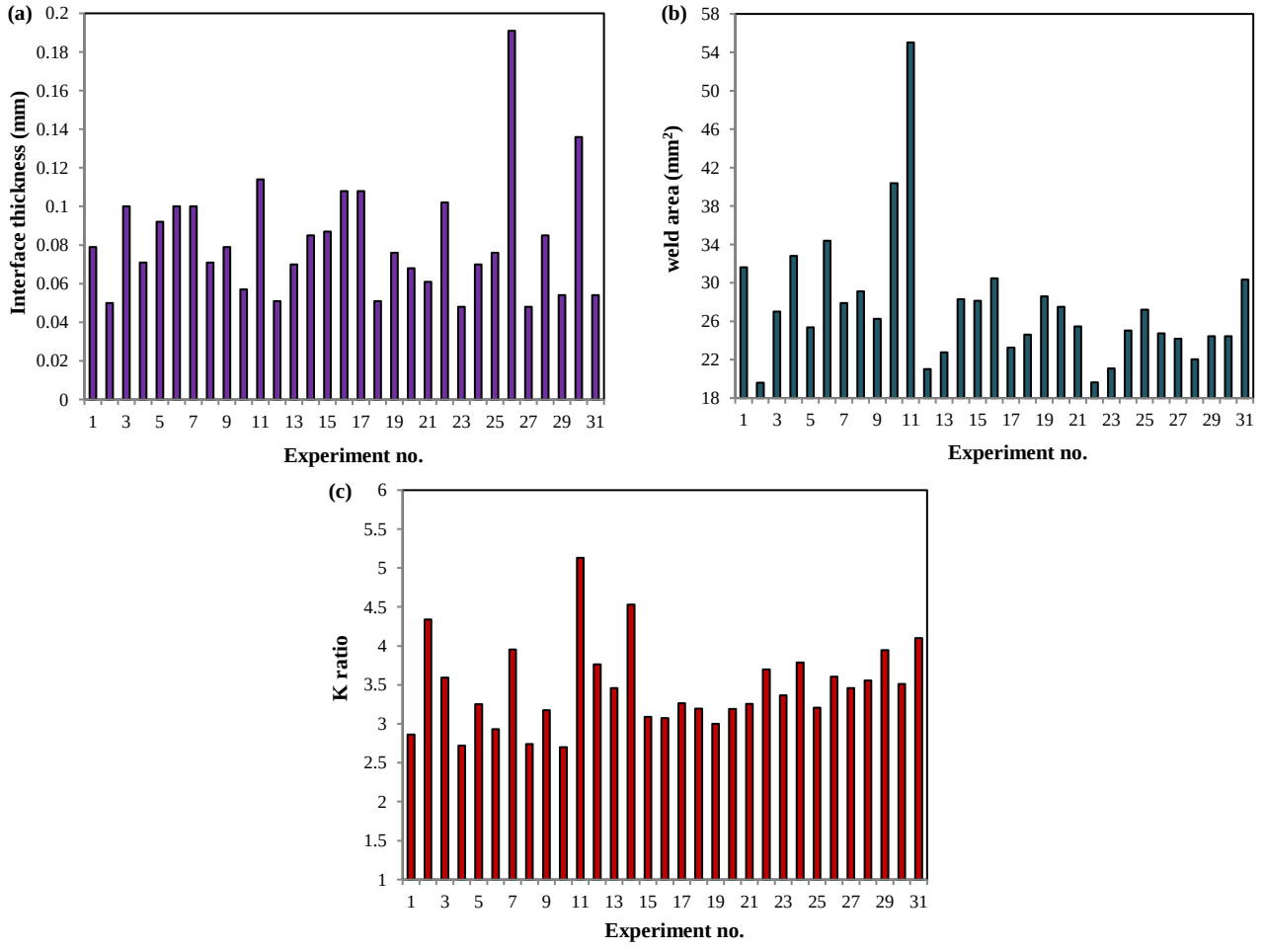

Figure 2. For all the experiments; interface thickness (a), Weld area observed (b), and K ratio (c).

3.1 Macro study

The macrographs of all 31 experiments are shown in Figure 3. The macro study reveals the bead, weldment, fusion zone, heat affected zone (HAZ) and cross-section of the clad layer as in the figure. No defects were found in the zones. The dilution of the cladding is well understood through the macrographs. In the figures, the weldment with cladding satellite-6 material zone, base alloy SS316L zone and the weld bead surface is shown. It is important to present all the macrographs as the experiments were done with different conditions and thus the morphology of weld bead and the interface varied. For instance, the weld bead is not the same for both experiments 1 and 2. When looking at the molten zone in the base metal, it was varying according to the changes in the welding conditions. For instance, molten zone in base metal was not the same for the experiment 1, 2 and 3 as in the macrographs. In those experiments, the torch angle and welding speed were common, but the current and the voltage are not the same first three experiments. The higher current value with low voltage reduces the weld zone area and the low voltage, low current with low welding speed increased the weld zone. The fusion line is shown in the image of experiment number 3. Thus, it was observed that the welding factors and their different values decide the size and shape of the weld bead and the HAZ. It can be further noted the bead width and bead height with the help of macrographs as mentioned in the image of experiment number 5. All the experiments had almost equal bead width. From the macrographs, amongst the experiments 4 to 9, the HAZ, and the bead height are higher than the others. From experiments 10 to 25, it was noted that the quantum of molten metal in base alloy is different. From the 25th experiment to the 31st experiment, the cladding performance shows almost the same.

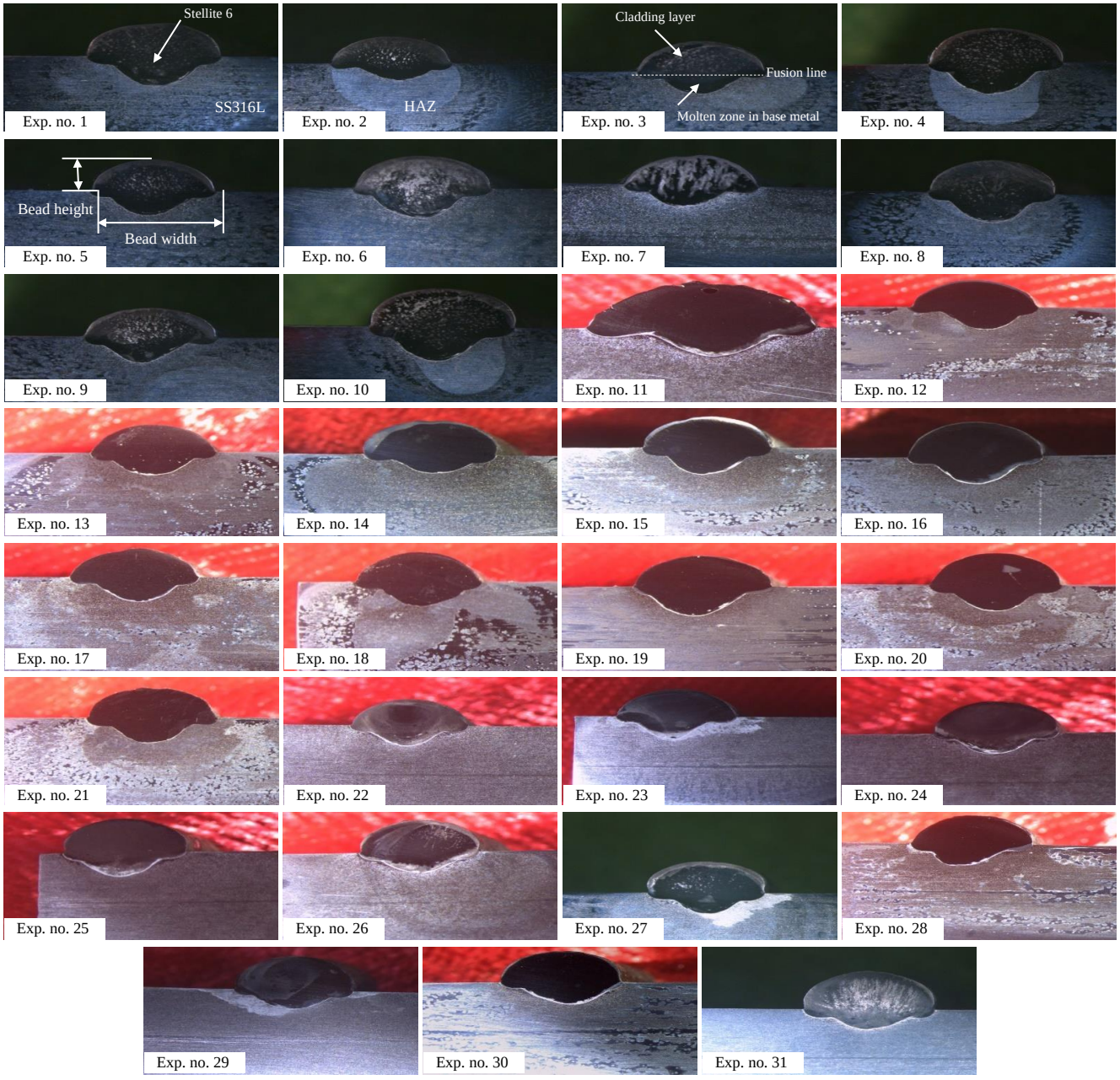

Figure 3. Macro images of weld bead for all the experiments (10×).

3.2 Micro characterization

The microstructures of the SS316L base alloy (without any surface modification and heat treatment) and the claddings are shown in Figure 4 and Figure 5, respectively. The austenitic structure grain is seen, which promotes the toughness property. Figures 5 (a-c) are showing the interfaces developed by the 2nd, 11th, and 26th experiments, respectively. The structures of cladding stellite-6, interface to fusion zone, and base alloy can be seen from the figures. The fine structure was obtained by the cladding process. The interface is seen in the figures between the satellite-6 weldment and the substrate SS316L, but the width is different. Figure 5(a) it was noted that the width of the interface thickness is very thin around 50 μm by the 2nd experiment of having a high current of 180 A. Figure 5(b) is the image of the interface that has 110 μm thick by the 11th experiment of having high current 180 A. Similarly, Figure 5(c) is the image of the 26th experiment; there the thickness of the dissimilar interface is about 190 μm. In the satellite-6 cladding side, the cobalt-rich dendrite structure can be seen nearby the interface. From the results, it cannot be judged about the influence of the welding factors on the interface thickness. The factors combination is important and to be optimized.

Figure 6 shows the optical micrographs of the cladding layer with satellite-6 for all the experiments (Exp. no. 1 to 31). The dendritic hard structure with a Co-rich phase is found almost in all the welds. A quantum of Co phase may be varying as seen in the microstructure according to the experimental conditions. Though the structure seems to be the same, the formation of the grains and the dendrites are different and they were depending on the welding factors combination and their values during the cladding process. The inter-dendrite structure of stellite metal has M_7C_3-carbides [12].

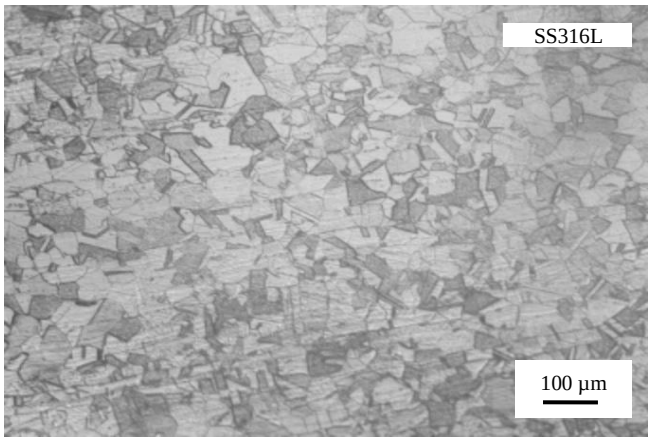

Figure 4. Microstructure of base SS316L (200×).

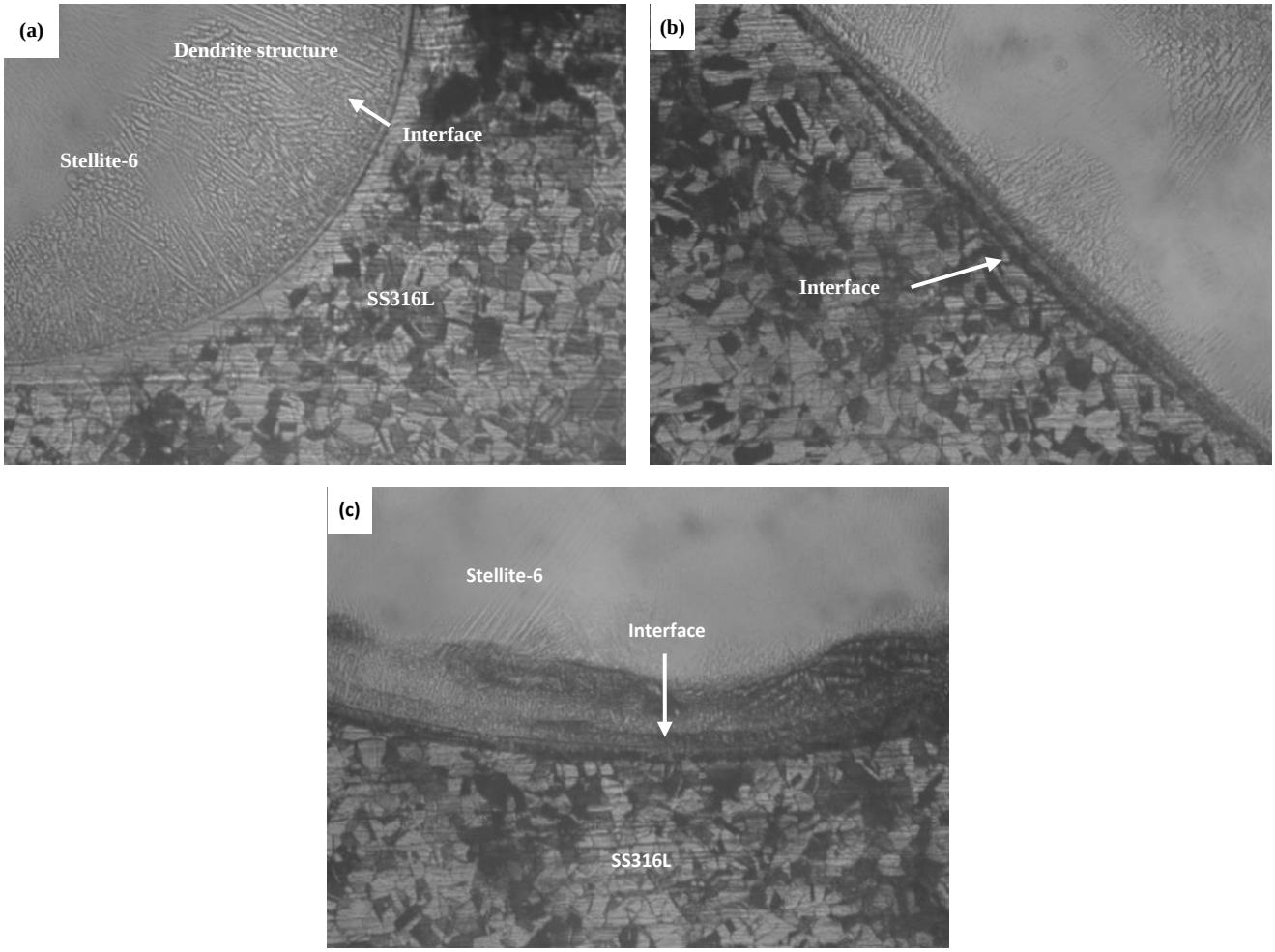

Figure 5. Microstructures of cladding interface (100×). (a) Exp. no 2, (b) Exp. no 11, and (c) Exp. no 26.

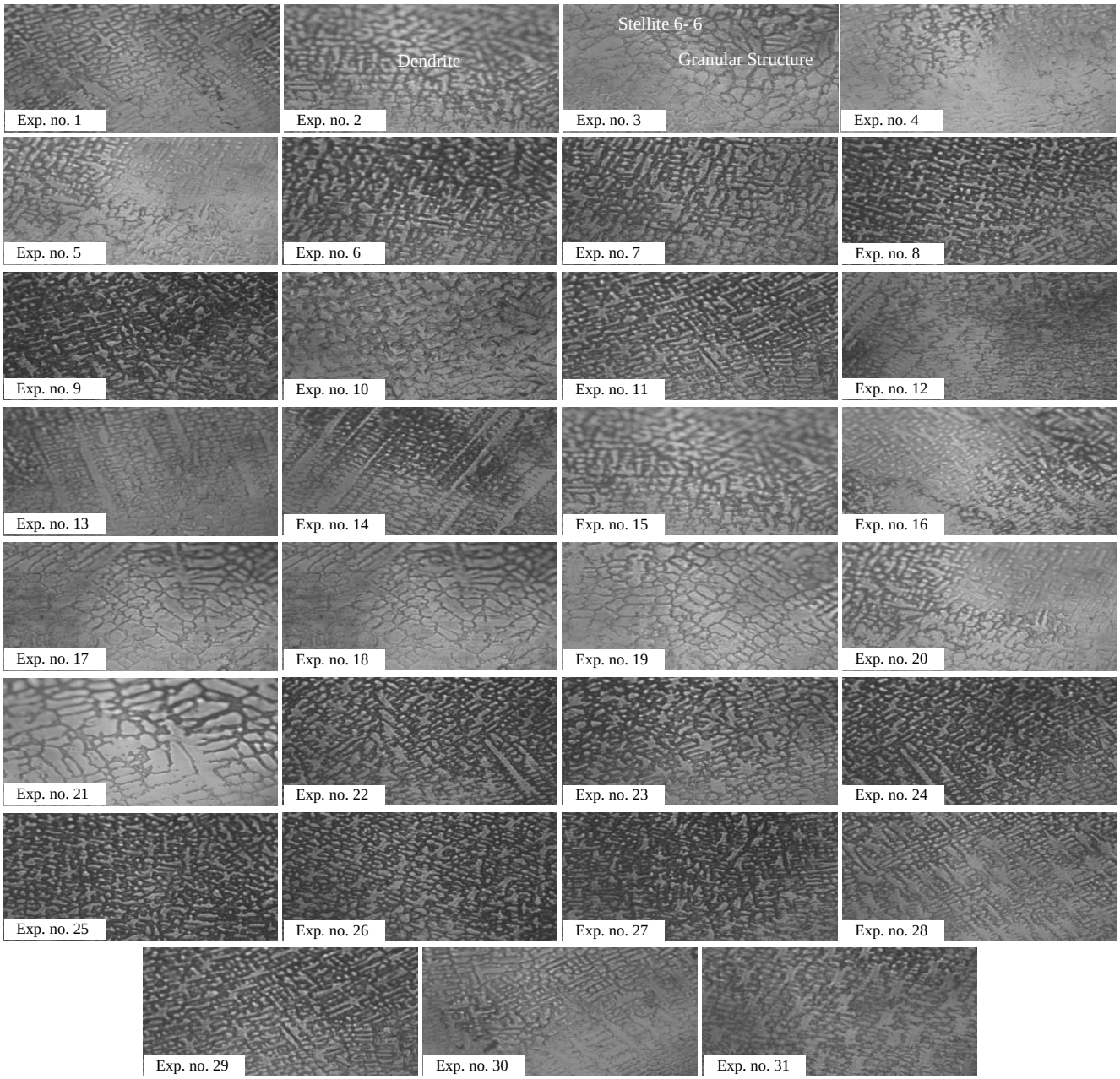

Figure 6. Microstructures of Stellite-6 cladding with 500× magnification.

Figures 7(a-c) are the SEM images showing weldment, interface and base metal regions developed by experiments 2, 11, and 26, respectively. According to the thickness of the interfaces in thin, medium and thick, the images are only considered here among the 31 experiments. Some striker lines are seen up to 60 μm distance from the interface line nearby the interface especially on the stellite-6 side as in Figure 7(b). The cobalt-rich phase structures are shown in Figures 7(c), (e) and (j). The HAZ zone in the molten metal zone of SS316L alloy is shown in Figure 7(e), these HAZs can be varied according to the changes in the values of welding parameters. The wall thickness of the phases in the stellite-6 region was almost the same and its average size was about 1 micron. From the structures, it can be well understood that the cladding was perfectly done on the surface of the SS316L alloy. Figures 7(h) shows good bonding and a strong interface.

3.3 EDX and XRD analysis

Figure 8 is the EDS point analysis at weld, interface and base metal. The points where the EDS had been taken are shown as a square in Figures 8(a-c). The EDX were analysed on the specimens, which had low, medium and high corrosion rates (i.e.) experiments 30, 7 and 19, respectively. It should be noted the chemical elements' changes in the interface and base alloy as they may be changed by different welding factors. Figures 8(d-i) reveal the material elements present in the portions like weld/stellite-6, interface and SS316L side in the cladding specimen. Figures 8(d-f) are the EDS spectrum of experiment number 30. On the weld side, the elements Fe was the major of 45% followed by Co and Cr. Similarly, in the interface and base metal, the Fe element was a higher weight of 55% followed by Cr and Co. Figures 8(g-i) are showing the EDS analysis of experiment number 7.

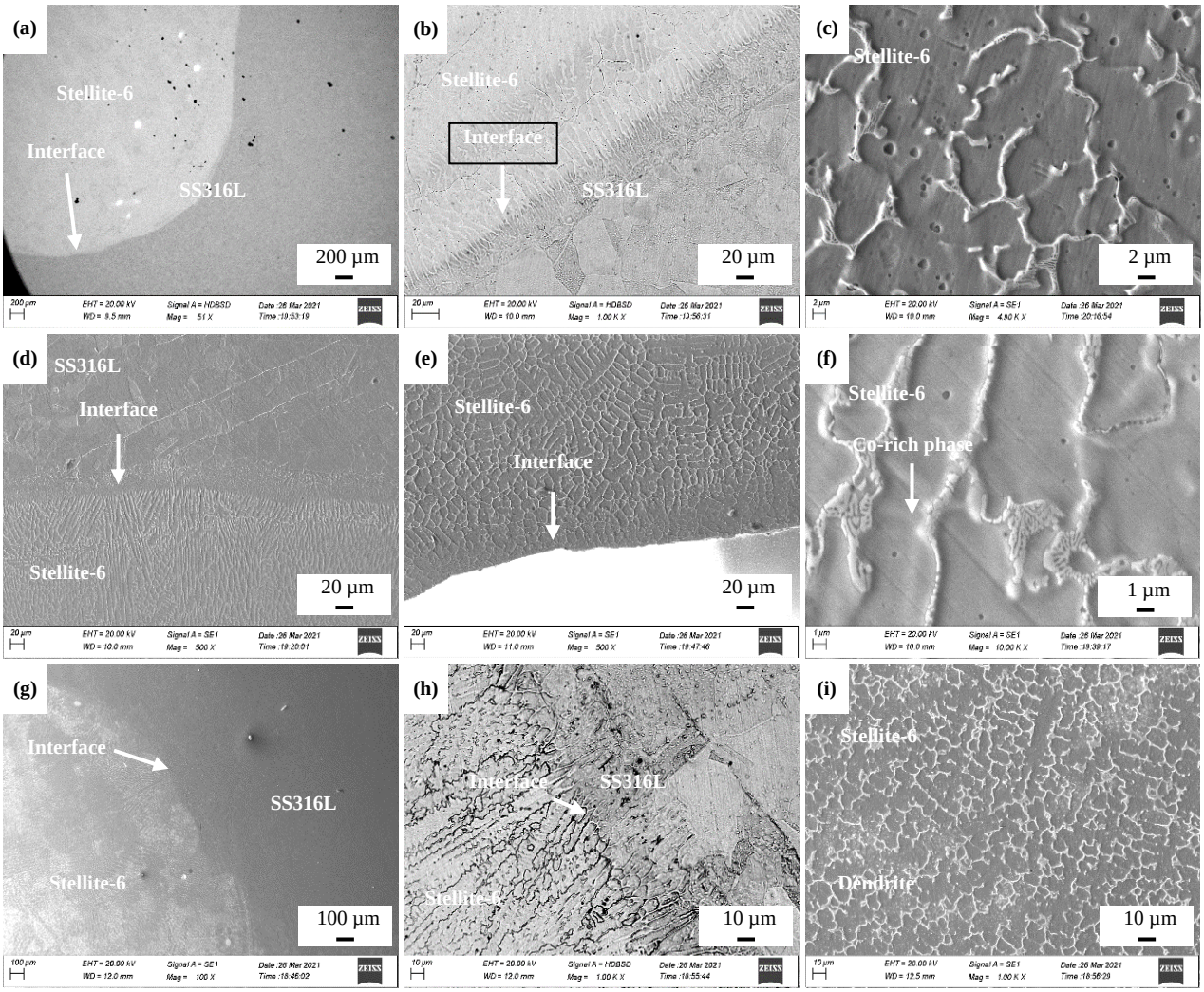

Figure 7. SEM images of cladding specimen. Where (a-c) Exp. no 2, (d-f) Exp. no 11, and (g-i) Exp. no 26.

A maximum of higher Fe element of 61% was found in the base metal side, but cobalt of 17% was higher at the stellite-6 weld zone followed by Fe and Cr. The interface had higher corrosion resistance. Figures 8(j-l) are the EDS spectrum of experiment 19 which had a higher corrosion rate. According to Figure 8(j), Co was higher at 36% followed by Fe and Cr at the weld. In the interface and SS316L base metal side, Fe higher was higher with around more than 50%. According to EDS, though Fe, Cr and Co were the major elements, their mass values were different. It can be noted that at the base metal, interface and stellite-6 weld were influenced only by Fe, Co and Cr elements.

Figures 9(a-c) are the colour elemental mapping of the specimens at the cladding satellite-6 side. The colour mapping was used to analyse the element distribution. The distribution of the elements Fe, Co etc is understood from Figures 9(a-c). The elements are uniformly distributed over the surface though the quantities of the element are varying. Almost Fe, Cr and Co elements are equally spread over. The XRD analysis nearby the interfaces on the specimens by the cladding experiments Experiment no. 1, 3, 4, 5, 8, 9, 10, 22, 24, and 30 are given in Figure 10(a) and Figure 10(b), respectively. The Cobalt rich phases, Fe and Cr are found in clad layer.

3.4 Corrosion Rate

Figures 11(a) and (b) show the SEM images of the corroded specimens. Mainly the base metal little bit corroded than the clad region. The analysed corrosion rates of the experiments are given in the plot, Figure 12. According to the analysis, experiments 19 followed by experiment 12 recorded peak corrosion rates per year as 0.087 mm/yr. and 0.084 mm/yr., respectively. While comparing both experiments 19, 12, it was noted that the combination of current, speed and voltage influenced the corrosion rate and produced maximum corrosion rate. The maximum current of 160 A, minimum welding speed and minimum voltage of 15 V yielded maximum corrosion rate as in experiment 19, whereas the maximum current of 180 A and a maximum voltage of 21 V as in experiment 12 also produced a higher corrosion rate. It was also noted that the minimum level of welding speed developed a low corrosion rate. Most of the experiments showed the corrosion rate between the low and medium values i.e. 0 to 0.03 mm/year.

Figures 13-15 discuss the SEM and EDS elemental analysis on the corroded specimens cladding using the welding conditions as in experiments 19 (high corrosion rate), 7 (medium corrosion rate)

and 30 (low corrosion rate). Figure 13(a) is the SEM image of the corroded specimen, from where the elements were analysed through EDS. The boxes in the images are pointing out the EDS analysed positions. The EDS was analyzed at different regions in the corroded area. From Figure 13(b), the specimen with a higher corrosion rate contains the elements majorly S, C, and with other elements like Cl, Si. Further, in some areas, the element O was also present. The EDS spectra showed that the maximum corroded area (Figure 13(d)) had more iron content and the amount of Cr and Co was less. The element O present was more than 7% in the corroded region. The presence of oxygen stimulated the corrosion. According to the Figure 13(c), the elements Co and Cr percentage was maximum and the low Fe than that of the highly corroded region. The low corroded region had the element O only 1%. Figures 14(a-d) are for the 7th experiment. The elements Co, Fe and Fe were the major elements and the quantity were 38%, 24% and 22%, respectively in the highly corroded region. Though the Fe and Cr content were the same in both high and low corroded regions, the Co content was higher of about 41% in the low corroded regions. The element O seems to be low in the low corroded regions.

From Figure 15, the element chlorine (Cl) was higher only in the high corrosion regions as per the EDS results. The presence of Cl was also seen in the SEM images (Figure 15(a) and (b)). Almost the mass of the Fe element was the same in the EDS position. Very few traces of the element S were found and the amount of Si element was also low in the low corroded region. It was understood that the Co-rich phase and the low content of element O are important and resist the corrosion on the specimen.

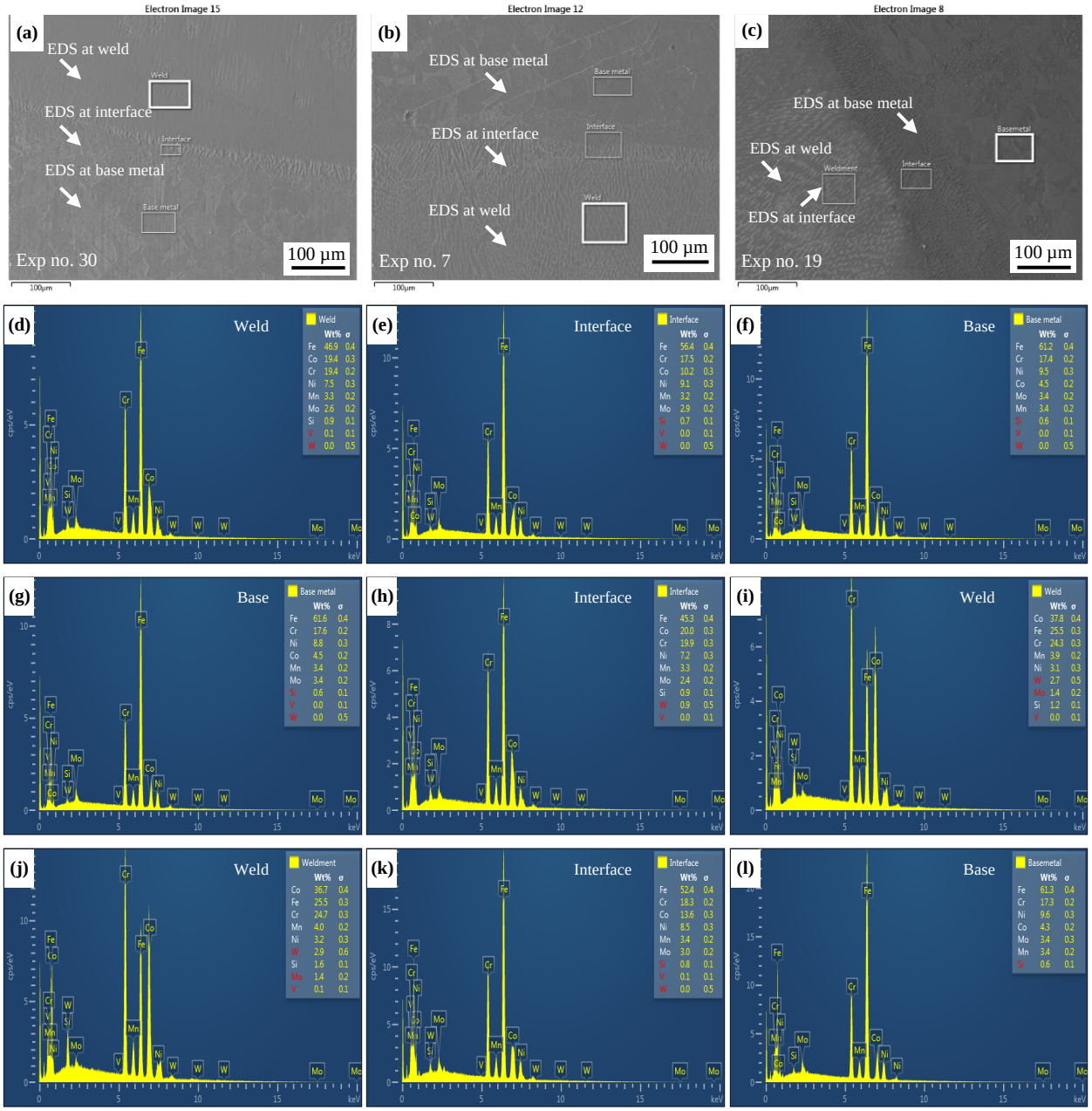

Figure 8. SEM of EDS analyzed positions and EDS spectra of specimen with low (images a, d-f: Exp. no. 30), medium (b, g-i: Exp. no. 7), and high corrosion rate (c, j-l: Exp. no. 19).

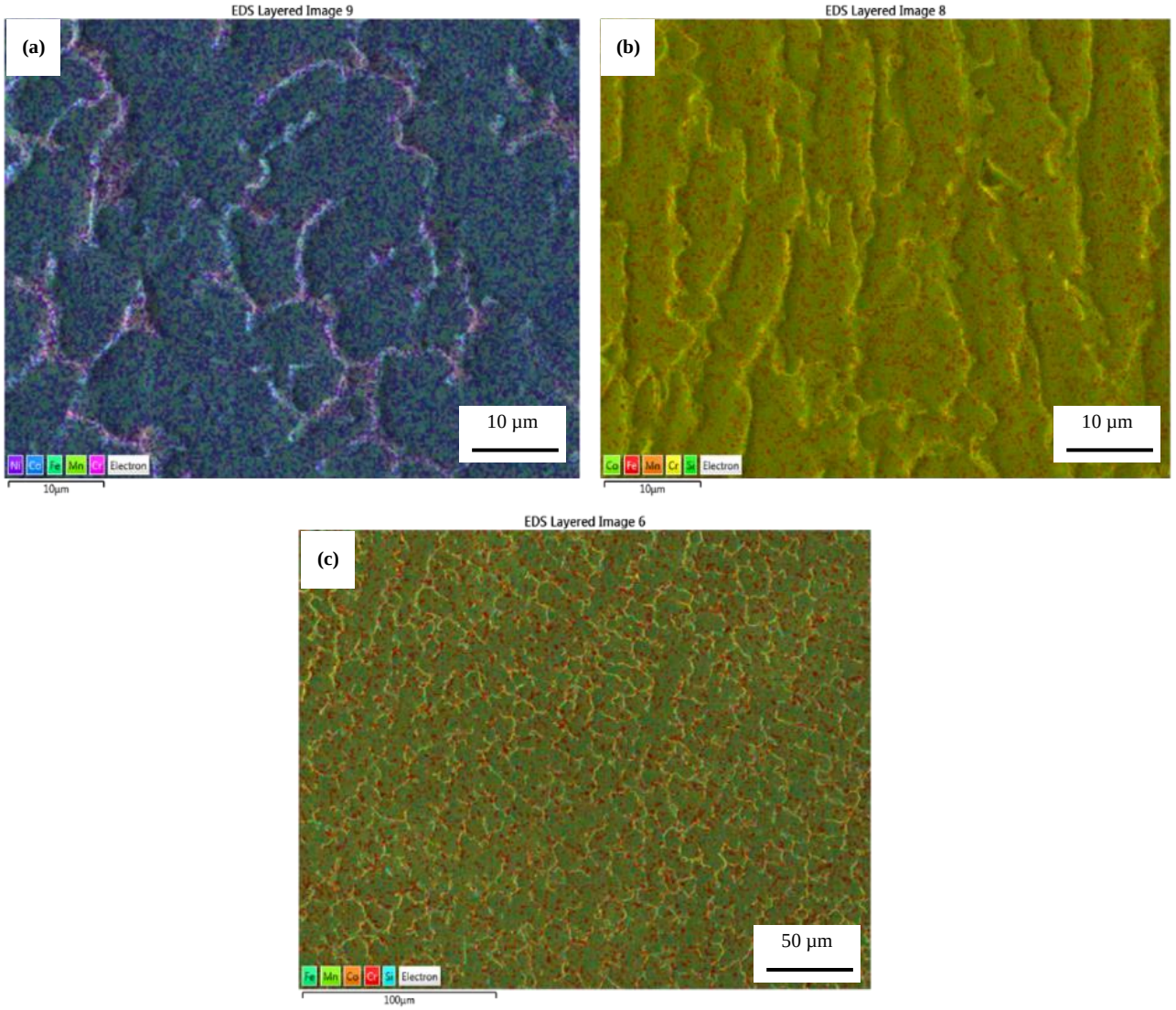

Figure 9. EDS color mapping of the specimen (images (a) Exp. no. 30, (b) Exp. no. 7, and (c) Exp. no. 19.

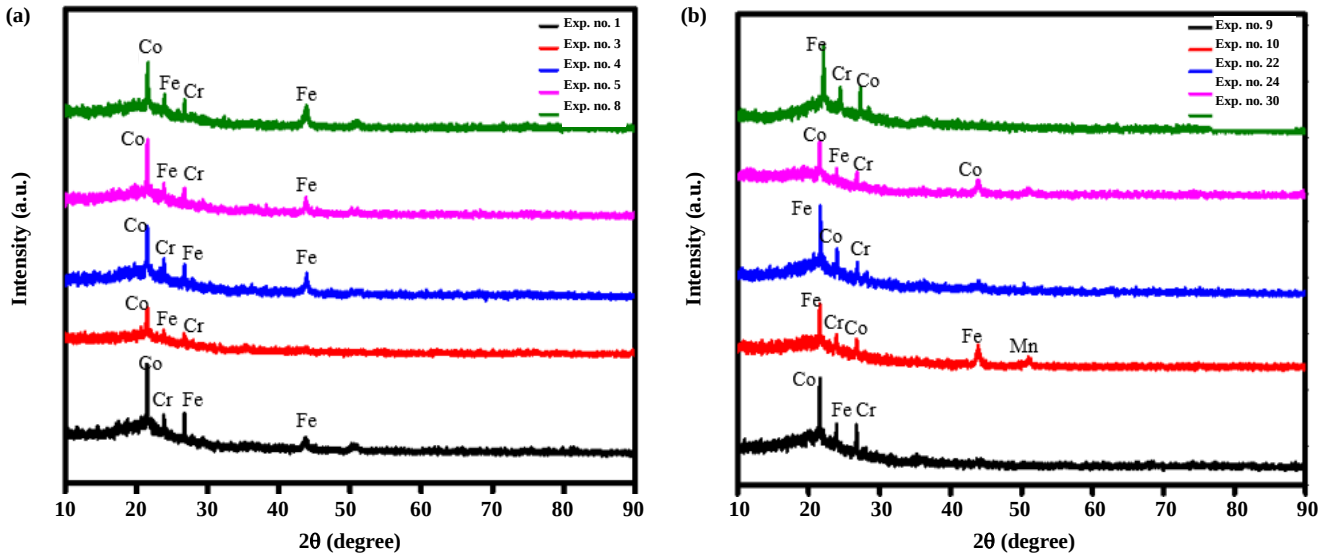

Figure 10. XRD report for the experiments (a) Exp. no. 1,3,4,5 and 8, and (b) Exp. no. 9,10,22,24 and 30.

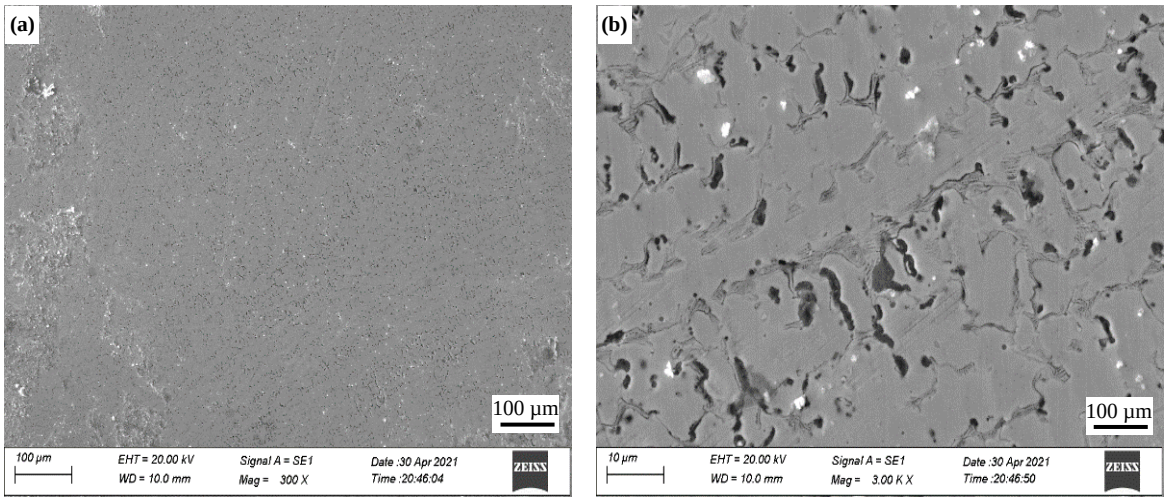

Figure 11. SEM image of corroded specimens (a) @300×, and (b) @3000×.

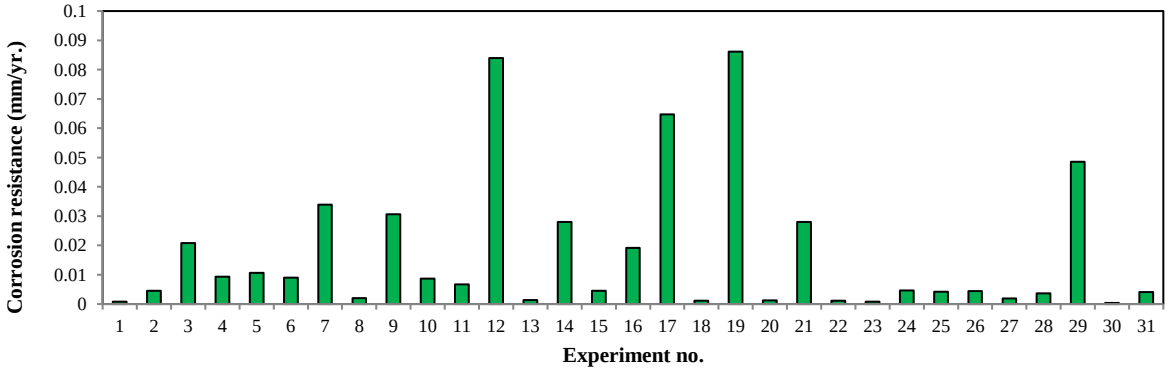

Figure 12. Corrosion rate per year analysis for all experiments.

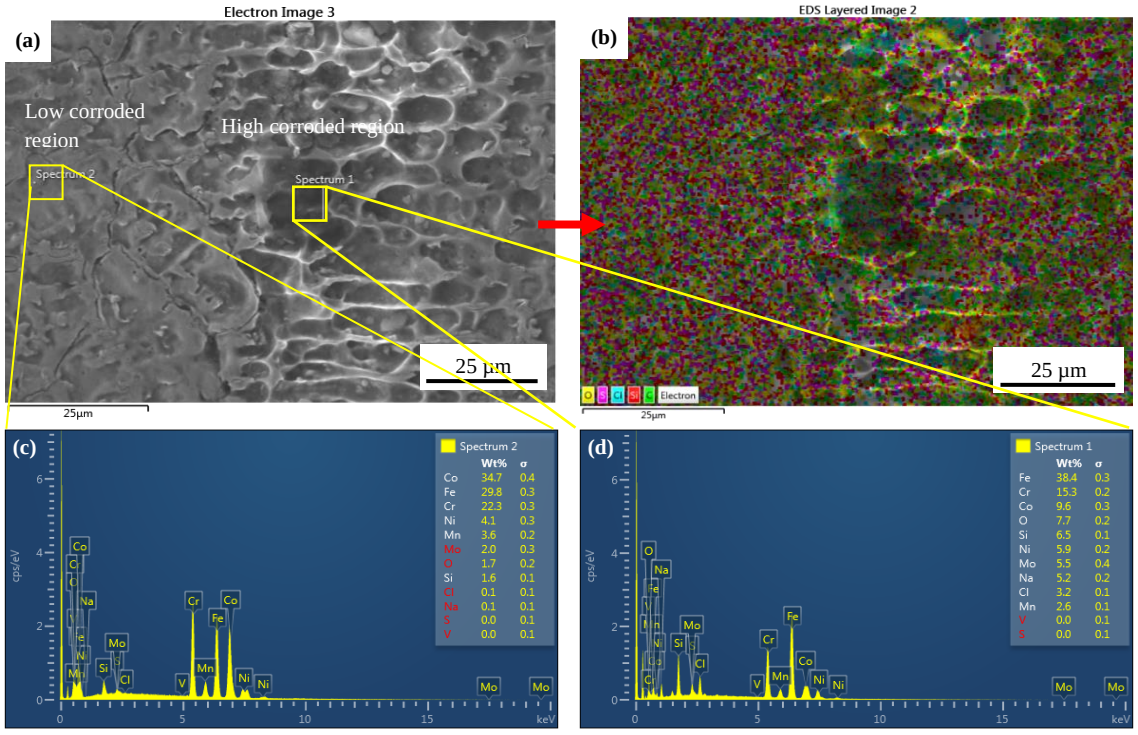

Figure 13. SEM image and color mapping on the corroded specimen Exp. no. 19 (a) SEM Image, (b) Color mapping, (c) EDAX at low corroded region, and (d) EDAX at high corroded region.

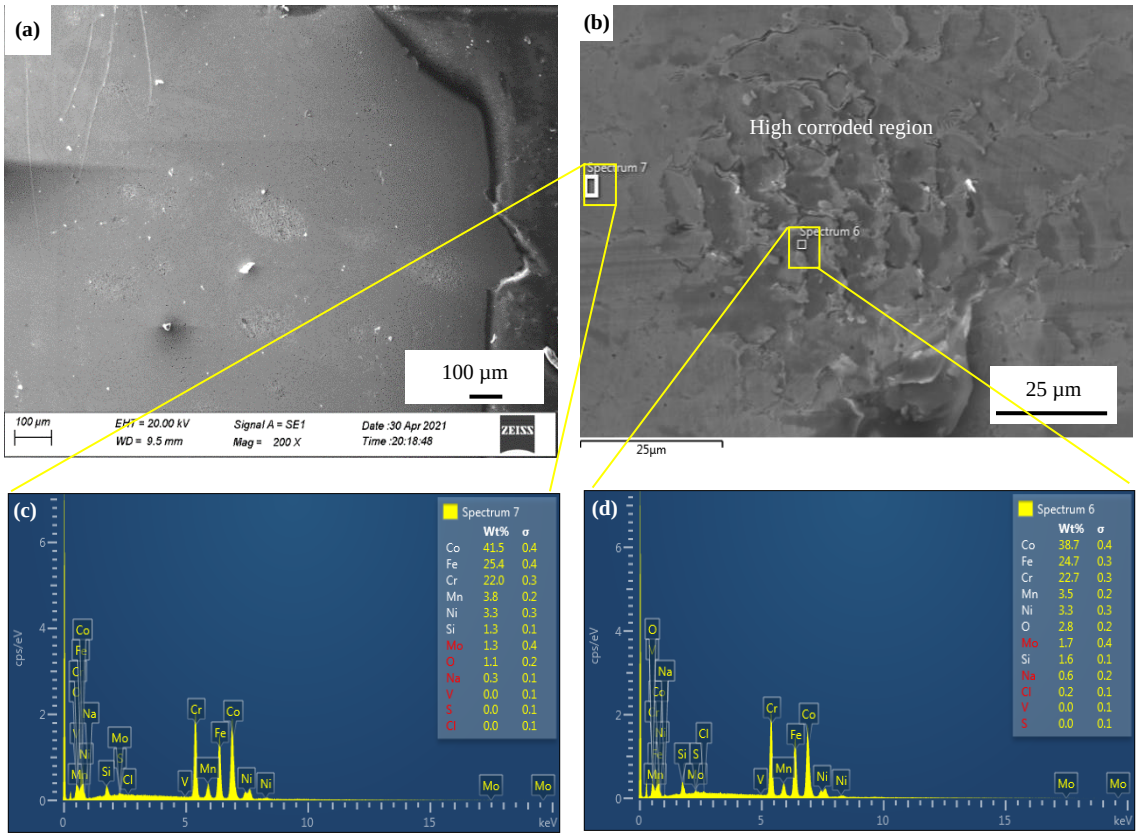

Figure 14. SEM image and color mapping on the corroded specimen Exp. no. 7 (a-b) SEM Image, (c) EDAX at low corroded region, and (d) EDAX at high corroded region.

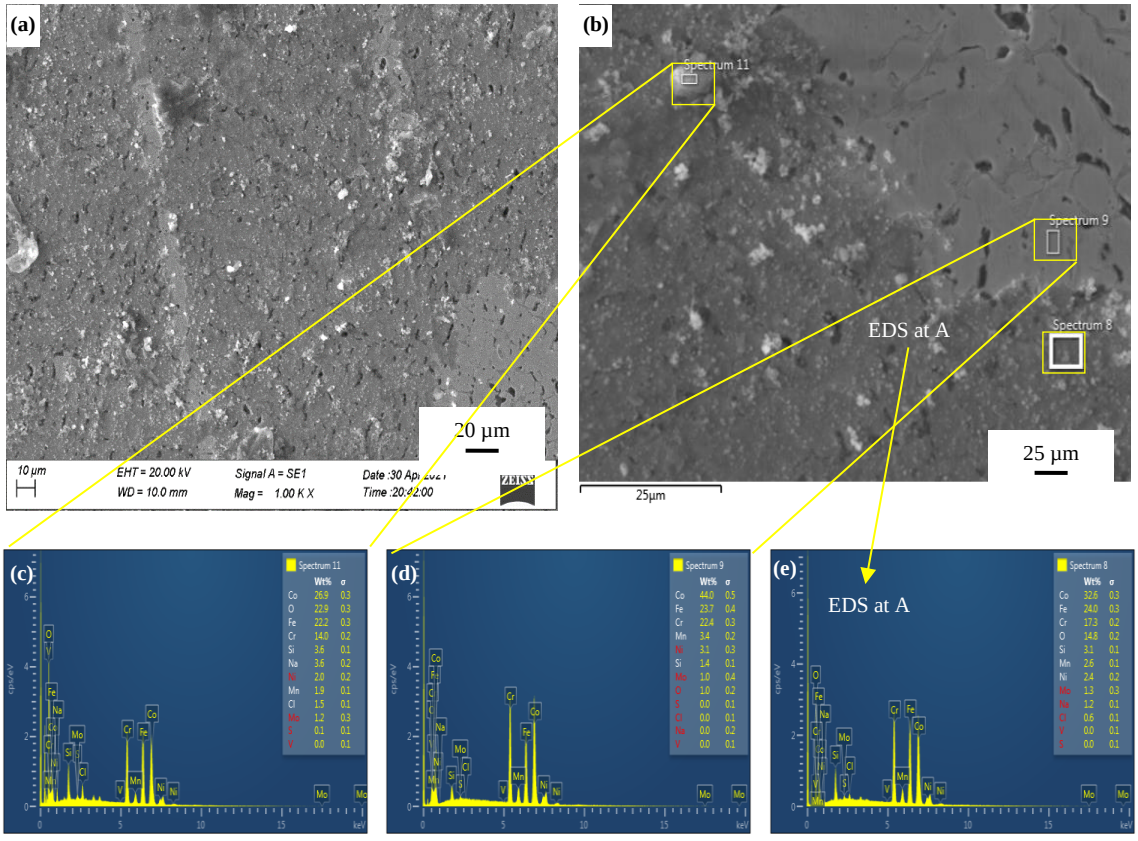

Figure 15. SEM image and color mapping of specimen after corrosion test Exp. no. 30 (a-b) SEM Image, (c, d, e) EDAX at corroded region.

3.5 Hardness of the Cladding

The microhardness values of all experiments were measured along the cladding weldment, weld interface and base metal SS316L using Vickers hardness tester under 1 kg load. The graph, Figure 16, is showing the evaluated microhardness for the three areas cladding, interface and SS316L. It is worth measuring the microhardness after the cladding process along the fusion zone nearby interface which decides the property of the welding conditions. From the hardness plot, it was noted that the hardness at the cladding weldment area was higher than the other area, which was around 1.25 times greater than that of interface's hardness and 2 times greater than that of SS316L regions. The maximum value of around 380 Hv1.0 at the interface was recorded for the 18th experiment with a high current of 200 A, whereas the hardness of the 18th experiment at the SS316L region with 175 Hv1.0 is not appreciable. The high current can resist the hardness property of the base metal by softening the surface during the cladding process. Almost all the experiment had hardness in the cladding region above 320 Hv0.1. From experiment no. 15, the hardness of interface and cladding region was better as the experiment was done with a higher 21 V, 80° torch angle and 175 m·min^{-1} welding speed, but at a low speed of 140 A. However, the welding factors with low values as in the 26th experiment showed poor hardness. From the results, it can be considered that the higher current values or the combination of higher welding speed with higher voltage provide excellent hardness on the Cladding side. The hardness at the interface was a maximum of 270 Hv1.0 for the 21st experiment. While comparing interface hardness for both 21st and 24th experiments, it can be noted that the welding speed played a major role as the increase in welding speed decreased the hardness. The combination of low current with high welding speed as in the 9th experiment yielded low hardness on the SS316L base metal side. Even though the welding conditions for experiments 23 to 31 are the same as per the CCD matrix, each trial on the weld specimens showed minor variations only.

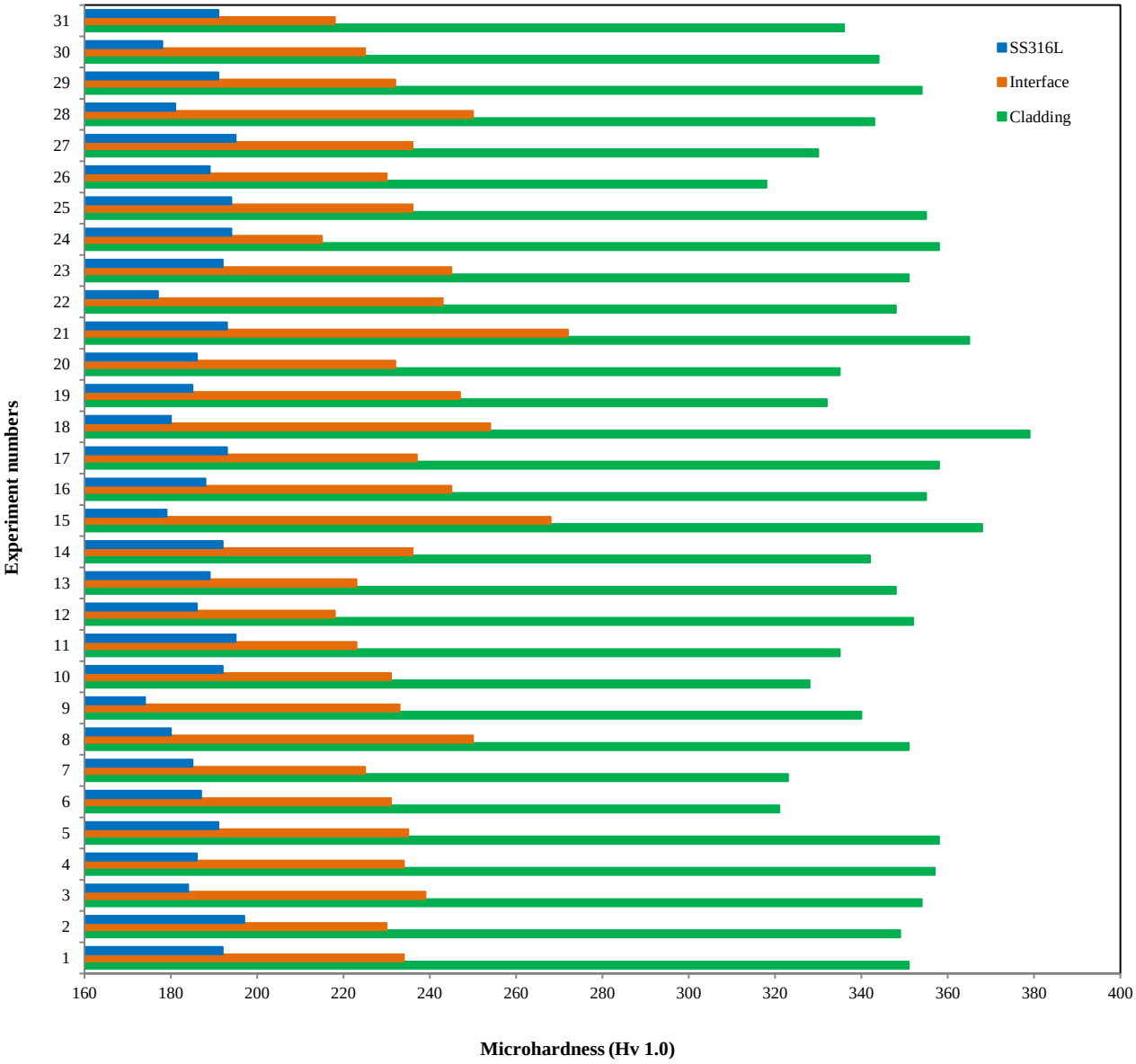

Figure 16. Microhardness measurement along metal SS316L, Interface, and Cladding areas.

4. Conclusions

In this work, Stellite-6 filler wire cladding was successfully done over the base metal SS3316L through the CMT process as per the CCD matrix. The specimens were characterized and the results were presented in this paper. The following conclusions are drawn as follows.

- Macro and microstructures study, EDS, XRD, corrosion study, Vickers microhardness were analysed at interface, SS316L base alloy, and stellite-6 regions were done using the sophisticated equipment. And weld area, K ratio, depth of penetration, the width of bead, face reinforcement, weld toe angle were evaluated.
- From macrographs, experiment with low welding speed, welding current and voltage yielded maximum molten zone of the base alloy.
- The thickness of the interface and the co-rich phase were varied according to the welding factors combinations. Higher torch angle with the combination of higher current stimulated to have thick interfaces.
- Experiment 25 to 31 experiment, the cladding performance was almost the same.
- A higher voltage of 21 V and high welding speed developed a large weld area.
- Higher current increased the depth of penetration.
- Experiment 11 of current 140 A, 21 V and weld speed 175 $m \cdot min^{-1}$ produced maximum bead width, maximum face reinforcement and maximum toe angle.
- The EDS analysis on the corroded specimens revealed the presence of Co rich and low content of O element in the low corroded regions.
- The weld by the experiment with minimum welding speed and minimum current yielded a low corrosion rate.
- In the case of microhardness, the welding current is important. The higher current increases hardness and while the low speed with low current decreases the hardness. Clad weldment portion has maximum hardness over the interface and base alloy.

Declarations

- Funding: This study was not funded by any organization.
- Conflicts of interest/Competing interests: The authors declare that they have no conflict of interest.
- Availability of data and material: All data and materials support their published claims and comply with field standards.

References

[1] H. So, C.T. Chen, and Y.A. Chen, "Wear behaviors of laser-clad stellite alloy 6," *Wear*, vol. 192, pp. 78-84, 1996.

[2] R. Jendrzejewski, C. Navas, A. Conde, J. J. de Damborenea, and G. Śliwiński "Properties of laser-cladded stellite coatings prepared on preheated chromium steel," *Materials & Design*, vol. 29, no. 1, pp 187-192, 2008.

[3] D. Bartkowski, A. Młynarczak, A. Piasecki, B. Dudziak, M. Gościański, and A. Bartkowska "Microstructure, microhardness and corrosion resistance of Stellite-6 coatings reinforced with WC particles using laser cladding," *Optics & Laser Technology*, vol. 68, pp. 191-201, 2015.

[4] A. Shahroozi, A. Afsari, B. Khakan, and A.R. Khalifeh "Micro-structure and mechanical properties investigation of Stellite 6 and Stellite 6/TiC coating on ASTM A105 steel produced by TIG welding process," *Surface and Coatings Technology*, vol. 350, pp. 648-658, 2018.

[5] Z. Zhang, F. Kong, and R. Kovacevic "Laser hot-wire cladding of Co-Cr-W metal cored wire," *Optics and Lasers in Engineering*, vol. 128, pp 105998, 2020.

[6] T. Gabriel, D. Rommel, F. Scherm, M. Gorywoda, and U. Glatzel "Laser cladding of ultra-thin nickel-based superalloy sheets," *Materials*, vol. 10, pp 279, 2017.

[7] K. Wang, H. Wang, G. Zhu, X. Zhu, "Cr13Ni5Si2-based composite coating on copper deposited using pulse laser induction cladding," *Materials*, vol. 10, pp 160, 2017.

[8] Y. Wuyan, L. Ruifeng, C. Zhaohui, G. Jiayang, and T. Yingtao, "A comparative study on microstructure and properties of traditional laser cladding and high-speed laser cladding of Ni45 alloy coatings," *Surface and Coatings Technology*, vol. 405, ISSN 0257-8972, 2021.

[9] S. K. Selvaraj, K. Srinivasan, J. Deshmukh, D. Agrawal, S. Mungilwar, R. Jagtap, and Y. C. Hu, "Performance comparison of advanced ceramic cladding approaches via solid-state and traditional welding processes, *A Review Materials*, vol. 13, pp 5805, 2020.

[10] G. P. Rajeev, M. Kamaraj, and S. R. Bakshi "Hardfacing of AISI H13 tool steel with Stellite 21 alloy using cold metal transfer welding process," *Surface & Coatings Technology*, vol. 326, no. Part-A, pp. 63-71, 2017.

[11] A. Gholipour, M. Shamanian, and F. Ashrafizadeh "Micro-structure and wear behavior of Stellite 6 cladding on 17-4 PH stainless steel," *Journal of Alloys and Compounds*, vol. 509, no. 14, pp. 4905-4909, 2011.

[12] G. R. Mirshekari, S. Daee, S. F. Bonabi, M. R. Tavakoli, A. Shafyei, and M. Safaei "Effect of interlayers on the micro-structure and wear resistance of Stellite 6 coatings deposited on AISI 420 stainless steel by GTAW technique," *Surfaces and Interfaces*, vol. 9, pp. 79-92, 2017.

[13] G. Xu, M. Kutsuna, Z. Liu, and K. Yamada "Comparison between diode laser and TIG cladding of Co-based alloys on the SUS403 stainless steel," *Surface and Coatings Technology*, vol. 201, no. 3-4, pp. 1138-1144, 2006.

[14] T. A. V. Kumaran, S. A. N. J. Reddy, S. Jerome, N. Anbarasan, N. Arivazhagan, M. Manikandan , M. Sathishkumar "Development of pulsed cold metal transfer and gas metal arc welding techniques on high-strength aerospace-grade AA7475-T761*," J. of Materi Eng and Perform,* vol. 29, no. 11 pp. 7270-7290, 2020.

[15] F. Brownlie, T. Hodgkiess, A. Pearson, and A. M. Galloway, "Effect of nitriding on the corrosive wear performance of a single and double layer Stellite 6 weld cladding," *Wear*, vol. 376-377, no. Part B, pp. 1279-1285, 2017.

[16] A. Kusmoko, D. Dunne, and L. Huijun, "Effect of heat input on Stellite 6 coatings on a medium carbon steel substrate by laser cladding," *Materials Today: Proceedings*, vol. 2, pp. 1747-1754, 2015.

[17] C. R. C. Lima, M. J. X. Belém, H. D. C. Fals, and C. A. D. Rovere "Wear and corrosion performance of Stellite 6 coatings applied by HVOF spraying and GTAW hotwire cladding," *Journal of Materials Processing Technology*, vol. 284, pp. 116734, 2020.

[18] D. Féron "Overview of nuclear materials and nuclear corrosion science and engineering." in *Woodhead Publishing Series in Energy*, Nuclear Corrosion Science and Engineering: Woodhead Publishing, 2012, pp. 31-56.

[19] R. Singh, D. Kumar, S. K. Mishra, and S. K. Tiwari "Laser cladding of Stellite 6 on stainless steel to enhance solid particle erosion and cavitation resistance," *Surface and Coatings Technology*, vol. 251, pp. 87-97, 2014.

[20] M. Zhong, W. Liu, K. Yao, J. C. Goussain, C. Mayer, and A. Becker, "Microstructural evolution in high power laser cladding of Stellite 6+WC layers," *Surface and Coatings Technology*, vol. 157, no. 2-3, pp. 128-137, 2002.

[21] F. Brownlie, C. Anene, T. Hodgkiess, A. Pearson, and A. M. Galloway "Comparison of hot wire TIG Stellite 6 weld cladding and lost wax cast Stellite 6 under corrosive wear conditions," *Wear*, vol. 404-405, pp. 71-81, 2018.

[22] P. Ganesh, A. Moitra, P. Tiwari, S. Sathyanarayanan, H. Kumar, S. K. Rai, R. Kaul, C. P. Paul, R. C. Prasad, and L. M. Kukreja "Fracture behavior of laser-clad joint of Stellite 21 on AISI 316L stainless steel," *Materials Science and Engineering: A*, vol 527, no. 16-17, pp. 3748-3756, 2010.

[23] S. Ramesh, R. Prabu, and E. Natarajan. "Experimental investigation on structure, wear and erosion resistance of SS316 substrate coated with TiC-Al_2O_3 nano composite by laser cladding," *High Temperature Material Processes*, vol. 22(1), pp. 63-71, 2018.

[24] J. Bayuo, M. A. Abukari, and K. B. Pelig-Ba, "Optimization using central composite design (CCD) of response surface methodology (RSM) for biosorption of hexavalent chromium from aqueous media," Appl *Water Sci*, vol. 10, pp. 135, 2020.

[25] B. Sadhukhan, N. K. Mondal, and S. Chattoraj. "Optimisation using central composite design (CCD) and the desirability function for sorption of methylene blue from aqueous solution onto Lemna major," *Karbala International Journal of Modern Science*, vol. 2, no. 3, pp. 145-155, 2016.

[26] H. Ahn, "Central composite design for the experiments with replicate runs at factorial and axial points," in Industrial Engineering, Management Science and Applications, M. Gen, K. Kim, X. Huang, Y. Hiroshi, (eds) 2015. Lecture Notes in Electrical Engineering, Springer, vol. 349, 2015.

[27] A. Nair, V. Ramji, R. D. Raj, and R. Veeramani "Laser cladding of Stellite 6 on EN8 steel – A fuzzy modelling approach," *Materials Today: Proceedings*, vol. 39, no. Part 1, pp 348-353, 2021.

[28] F. Madadi, F. Ashrafizadeh, and M. Shamanian "Optimization of pulsed TIG cladding process of stellite alloy on carbon steel using RSM," *Journal of Alloys and Compounds*, vol. 510, no. 1, pp. 71-77, 2012.

[29] A. Asghar, A. A. A. Raman, and W. M. A. W. Daud, "A comparison of central composite design and taguchi method for optimizing fenton process," *The Scientific World Journal*, vol. 2014, Article ID 869120, p. 14, 2014.

[30] S. Bhattacharya "Central composite design for response surface methodology and its application in pharmacy" [Online First], *IntechOpen*, 2021.

[31] S. Ramesh, S. B. Boppana, and A. Manjunath, "Corrosion behavior studies and parameter optimization of dissimilar alloys joined by electron beam welding," *Journal of Bio- and Tribo-Corrosion*, vol. 6, pp. 73, 2020.